AGU PUBLICATIONS

JGR

Journal of Geophysical Research: Space Physics

RESEARCH ARTICLE
10.1002/2017JA023952

Survey of magnetic reconnection signatures in the Martian magnetotail with MAVEN

Y. Harada[1], J. S. Halekas[2], J. P. McFadden[1], J. Espley[3], G. A. DiBraccio[3,4], D. L. Mitchell[1], C. Mazelle[5,6], D. A. Brain[7], L. Andersson[7], Y. J. Ma[8], D. E. Larson[1], S. Xu[1], T. Hara[1], S. Ruhunusiri[2], R. Livi[1], and B. M. Jakosky[7]

[1]Space Sciences Laboratory, University of California, Berkeley, California, USA, [2]Department of Physics and Astronomy, University of Iowa, Iowa City, Iowa, USA, [3]NASA Goddard Space Flight Center, Greenbelt, Maryland, USA, [4]Universities Space Research Association, Columbia, Maryland, USA, [5]CNRS, IRAP, Toulouse, France, [6]IRAP, Université Paul Sabatier, Toulouse, France, [7]Laboratory for Atmospheric and Space Physics, University of Colorado Boulder, Boulder, Colorado, USA, [8]Institute of Geophysics and Planetary Physics, UCLA, Los Angeles, California, USA

Key Points:
- First extended survey of comprehensive in situ reconnection signatures in the Martian magnetotail
- Reconnection occurs preferentially in the $-E$ hemisphere of the near-Mars magnetotail
- Reconnection could operate for at least 1–10% of the time in the Martian magnetotail

Correspondence to:
Y. Harada,
haraday@ssl.berkeley.edu

Citation:
Harada, Y., et al. (2017), Survey of magnetic reconnection signatures in the Martian magnetotail with MAVEN, *J. Geophys. Res. Space Physics*, *122*, doi:10.1002/2017JA023952.

Received 25 JAN 2017
Accepted 27 MAR 2017
Accepted article online 29 MAR 2017

Abstract We conduct an extended survey of reconnection signatures observed in the Martian magnetotail by the Mars Atmosphere and Volatile EvolutioN (MAVEN) mission. Although it is well established that magnetic reconnection plays a fundamental role in the dynamics of *intrinsic* magnetospheres, the role of reconnection in the dynamics of *induced* magnetospheres remains poorly understood. Based on comprehensive plasma and field measurements by MAVEN in the Martian magnetotail, we first identified 776 current sheet crossings and then selected 34 crossings with Hall magnetic field signatures, which are indicative of the ion diffusion region of tail reconnection. For the majority of the identified Hall field events, we observe ion flow enhancements in the directions consistent with the reconnection outflow directions expected from the Hall magnetic field polarity. The reconnection signatures are preferentially observed in the $-E$ hemisphere of the near-Mars magnetotail at ~1–2 Mars radii downstream from Mars. We have found no strong correlation of the likelihood of observing reconnection signatures with local crustal field strengths or with upstream drivers. The duty cycle of tail reconnection is estimated to be ~1–10% or even higher. The MAVEN observations suggest that magnetic reconnection can play an important role in the dynamics of the Martian magnetotail.

1. Introduction

Magnetic reconnection is a fundamental process operating in many regions of space plasmas. At magnetized planets with global dynamo fields, reconnection between solar and planetary magnetic fields and/or within planetary fields plays a central role in the dynamics of the intrinsic magnetospheres [e.g., *Dungey*, 1961; *Russell*, 2001; *Southwood*, 2015]. At unmagnetized planets such as Mars and Venus, the role of reconnection in the dynamics of the induced magnetospheres remains inconclusive [e.g., *Dubinin and Fraenz*, 2015; *Vech et al.*, 2016]. At comets, it was proposed that remotely observed tail disconnections can be caused by reconnection on the dayside ionospheres or in the nightside magnetotails [*Niedner Jr. and Brandt*, 1978; *Russell et al.*, 1986]. As the magnetotail provides one of the major pathways through which planetary ions escape from Mars [e.g., *Brain et al.*, 2010a; *Lundin*, 2011; *Dubinin et al.*, 2012a], understanding of the dynamics of the Martian magnetotail and physical processes operating therein is a critical step toward determining the atmospheric loss to space.

Magnetic reconnection at Mars was studied by utilizing in situ measurements of Hall magnetic fields and electrons from Mars Global Surveyor (MGS) [*Eastwood et al.*, 2008; *Halekas et al.*, 2009]. However, only limited spatial regions in the near-Mars space were explored by MGS owing to its orbit configuration at a fixed local time (2 A.M./2 P.M.) and altitude (400 km). For example, MGS never visited the center of the near-Mars magnetotail, where reconnection is expected to take place between the antiparallel lobe fields [e.g., *Eastwood and Kiehas*, 2015]. The previous Mars missions, including MGS and Mars Express, could not directly identify Alfvénic accelerated plasma flows within reconnecting current sheets because of the lack of adequate instrumentation. Such accelerated plasma flows within current sheets are considered as the clearest detectable signatures of

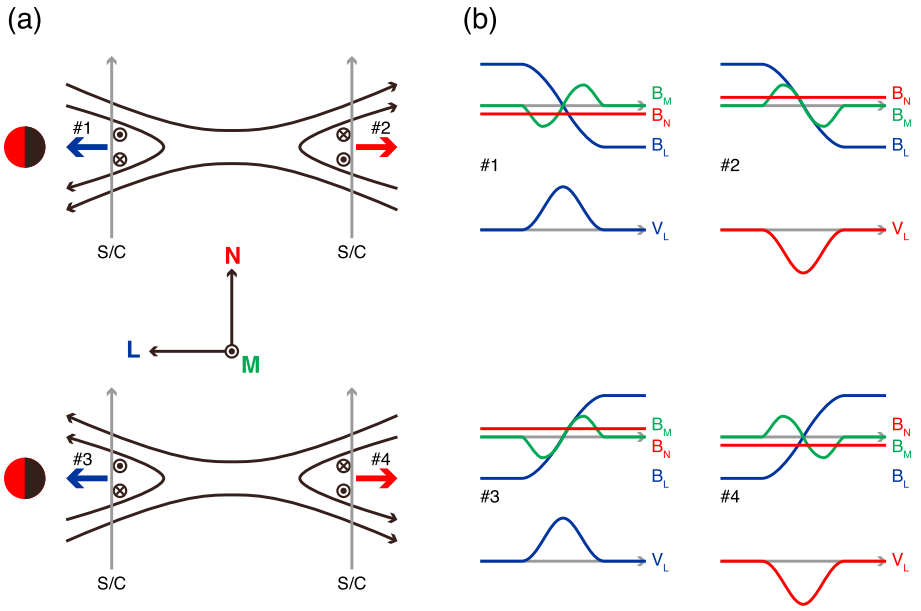

Figure 1. Schematic illustration of (a) possible geometries for spacecraft crossings of a reconnecting current sheet with Hall magnetic fields in the Martian magnetotail and (b) expected time series of the magnetic field and plasma flow velocity in the minimum variance *LMN* coordinate system. Here the polarity of the *LMN* coordinate system is chosen so that the maximum variance *L* direction has a sunward component and the minimum variance *N* direction points toward the spacecraft velocity vector in the rest frame of the current sheet.

magnetic reconnection [*Paschmann et al.*, 2013]. Local processes of particles and fields near the reconnection site in the Martian magnetotail as well as their global consequences remain poorly understood.

In addition to the direct measurements of the reconnection signatures in the vicinity of X lines, a number of observations demonstrate the presence of electron dynamics and magnetic field structures which could be the products of magnetic reconnection. Injection and trapping of electrons on closed magnetic field lines have been observed near the Martian crustal magnetic fields [*Brain et al.*, 2007; *Ulusşen and Linscott*, 2008; *Harada et al.*, 2016; *Xu et al.*, 2016]. Magnetic flux ropes can be formed by reconnection between draped interplanetary fields in the induced tail current sheets, between crustal and draped fields, or between neighboring crustal fields [*Brain et al.*, 2010b; *Briggs et al.*, 2011; *Beharrell and Wild*, 2012; *Eastwood et al.*, 2012; *Hara et al.*, 2014, 2016; *Soobiah et al.*, 2014; *DiBraccio et al.*, 2015]. In order to evaluate the role of reconnection in their generation processes, it is necessary to characterize the basic properties of magnetic reconnection at Mars based on in situ observations of particle and field signatures around X lines.

Comprehensive plasma and field measurements by the Mars Atmosphere and Volatile EvolutioN (MAVEN) mission [*Jakosky et al.*, 2015] have enabled direct investigation of ion, electron, and magnetic field signatures of magnetic reconnection with a wide coverage of spatial regions in the near-Mars space. *Harada et al.* [2015a] presented a case study on reconnection signatures observed within the central tail current sheet in the near-Mars magnetotail. The observed signatures include Marsward (sunward) acceleration of ion flows, Hall magnetic fields, and trapped electrons on closed field lines. In this paper, we conducted an extended survey of reconnection signatures in the Martian magnetotail with the aim of characterizing their individual and statistical properties. We first show case studies to examine the detailed characteristics of individual events. We then present statistical results of reconnection signatures identified from the available MAVEN data. We investigate basic characteristics of the reconnection events such as their spatial distributions, dependence on upstream drivers, and occurrence frequency, which would provide valuable information for the evaluation of the role of magnetic reconnection in the magnetotail dynamics and ion escape processes at Mars.

2. Expected Magnetic Field and Plasma Flow Signatures

Decoupling of ions and electrons in the ion diffusion region of collisionless magnetic reconnection leads to Hall currents, which produce quadrupole Hall magnetic fields around the ion diffusion region [e.g., *Pritchett*, 2001; *Yamada et al.*, 2010]. Figure 1a illustrates possible geometries of a crossing of a reconnecting current

sheet near the ion diffusion region by a spacecraft in the current sheet *LMN* coordinate system. In the *LMN* system, *L* is along the antiparallel magnetic fields (corresponding to the maximum variance direction obtained from the minimum variance analysis (MVA) of magnetic fields [*Sonnerup and Cahill*, 1967]), *M* is along the X line (intermediate variance direction), and *N* is along the current sheet normal (minimum variance direction). Here we choose the polarity of the *LMN* system by ensuring positive dot products between the *L* direction and the Sun direction and between the *N* direction and the relative spacecraft velocity direction. The out-of-plane Hall magnetic fields are observed as a bipolar variation in the time series of B_M (Figure 1b). Depending on the crossing geometry, the spacecraft observes one of the four patterns of field variations (types 1–4 in Figure 1). Types 1 and 3 (types 2 and 4) correspond to crossings sunward (tailward) of the X line. By appropriately choosing the polarity of the *LMN* system, we can infer the direction of the X line location based on the patterns of magnetic field variations.

Meanwhile, magnetic reconnection produces a pair of oppositely directed plasma flows ejected away from the X line (blue and red arrows in Figure 1a). These reconnection outflows are observed as plasma flow enhancements in the $\pm L$ direction during the current sheet crossings (Figure 1b). The spacecraft observes a sunward (tailward) flow enhancement for a crossing sunward (tailward) of the X line. Thus, in addition to the Hall magnetic field signatures, plasma flow enhancements provide independent information on the direction of the X line location.

In this paper, we first search for Hall magnetic field signatures to identify potential crossings of the ion diffusion region. We then investigate plasma flow signatures during the identified crossings. In this way, we can test the consistency between the magnetic field and ion flow signatures in the ion diffusion region of magnetotail reconnection at Mars.

3. Data

The main plasma and field data used in this paper were obtained by MAVEN during 2332 orbit segments within the geometric shadow ($X_{MSO} < 0$ and $\rho_{MSO} \equiv \sqrt{Y_{MSO}^2 + Z_{MSO}^2} < 1R_M$, thereby focusing on the tail region) at altitudes greater than 250 km (which is well above the nominal exobase at ~200 km altitude, thereby focusing on the collisionless plasma regime) from 30 November 2014 to 24 September 2016. The Mars Solar Orbital (MSO) frame is defined in such a way that the *X* axis points from Mars toward the Sun, *Y* points opposite to the direction of Mars' orbital velocity component perpendicular to *X*, and *Z* completes the orthogonal coordinate set. Specifically, we analyze time series data of magnetic fields from magnetometer (MAG) [*Connerney et al.*, 2015], ion velocities from SupraThermal And Thermal Ion Composition (STATIC) [*McFadden et al.*, 2015], and electron energy/pitch angle distributions from Solar Wind Electron Analyzer (SWEA) [*Mitchell et al.*, 2016].

Given the large thermal-to-bulk speed ratio of electrons in the Martian magnetotail, it is very difficult, if not impossible, to retrieve reliable electron bulk velocities from direct electron measurements by SWEA. Therefore, we only use ion measurements to investigate plasma flows produced by reconnection in the Martian magnetotail. We compute ion bulk velocities of three most-abundant species (i.e., H^+, O^+, and O_2^+) from four-dimensional (energy-azimuthal angle-elevation angle-mass) STATIC data products. As we use the ion data obtained in the high-altitude shadow region, spacecraft potential correction is conducted using negative spacecraft potentials estimated from the low-energy cutoff of ion energy spectra. The negatively charged spacecraft in shadow attracts the ambient low-energy ions, leading to STATIC's measurement of the ion energy spectrum including the low-energy ions with a distinct cutoff corresponding to the spacecraft potential. The spacecraft velocity is taken into account when computing the ion velocities in the Mars rest frame. To account for effects of STATIC's incomplete field of view (FOV), we compute a FOV quality flag for each species defined as the ratio of the solid angle of the unblocked FOV within a cone around $\mathbf{V}_b$ with an angular width of $\mathrm{atan}(V_{th}/|\mathbf{V}_b|)$, where $\mathbf{V}_b$ and V_{th} are the computed bulk velocity and thermal speed, respectively, with respect to the solid angle of the cone itself. The FOV flag of 1 means that the main population of the species is well within the clear FOV, and it becomes smaller as the main population approaches the FOV edge and parts of the population exit the FOV. If the FOV flag is smaller than 0.7 or the density is lower than 0.1 cm^{-3} (when the bulk velocity often becomes noisy due to poor counting statistics), we classify the velocity measurement as "less reliable." We study ion flow enhancements based only on the remaining "relatively reliable" ion velocity measurements.

We also use upstream driver measurements from Solar Wind Ion Analyzer (SWIA) [*Halekas et al.*, 2015], MAG, and Extreme Ultraviolet Monitor (EUVM) [*Eparvier et al.*, 2015] to infer the upstream conditions for the

observations conducted in the magnetotail. Information on the upstream solar wind and interplanetary magnetic field (IMF) conditions (such as the solar wind density, N_{SW}, velocity, $\mathbf{V}_{SW}$, proton temperature, $T_{p,SW}$, and IMF, $\mathbf{B}_{SW}$) is necessary to investigate how the upstream drivers control processes operating in the magnetotail and to organize tail measurements in the coordinate system relevant to the Mars-solar wind interaction, i.e., Mars Solar Electric (MSE) coordinates. In MSE coordinates, $+X$ points from Mars toward $-\mathbf{V}_{SW}$, $+Z$ is parallel to $\mathbf{E}_{SW} = -\mathbf{V}_{SW} \times \mathbf{B}_{SW}$, and Y completes the orthogonal coordinate set. Based on the SWIA and MAG measurements, undisturbed solar wind intervals are automatically selected by the algorithm described in section 3.1 of *Halekas et al.* [2016]. Then we compute orbit averages of the upstream parameters. To estimate the upstream conditions at the time when MAVEN is located in the magnetotail, we perform linear interpolation in time of the orbit-averaged upstream parameters taken immediately before and after the tail crossing. We conduct this interpolation only if the average upstream parameters of the two back-to-back orbits are both available. As for the coordinate transformation from MSO to MSE, we use the solar wind speed from SWIA to take aberration into account, and then we rotate the Y-Z plane by using the IMF direction measured by MAG.

4. Case Studies

In this section, we present case studies of reconnecting current sheet crossings to demonstrate how the expected magnetic field and ion velocity signatures of Figure 1 are compared to the MAVEN observations.

4.1. Crossing Sunward of the X Line

Figure 2 shows an example of a Hall magnetic field event consistent with a crossing sunward of the X line. We observe a current sheet crossing at 19:18 UT identified by a reversal in B_x and a decrease in $|\mathbf{B}|$ (Figure 2a). The induced-to-total field ratio, $|\mathbf{B} - \mathbf{B}_c|/|\mathbf{B}|$, where $\mathbf{B}$ is the magnetic field vector measured by MAG and $\mathbf{B}_c$ is the crustal magnetic field computed from the spherical harmonic model [*Morschhauser et al.*, 2014], indicates ~1 throughout the interval. This suggests that the Martian crustal field is not directly implicated in forming this current sheet. The dot product between the normalized magnetic field vectors before and after the crossing approaches −1 (Figure 2c), meaning that the current sheet is characterized by a large magnetic field rotation of $\sim 180^\circ$ with nearly antiparallel lobe fields.

In Figure 2e, we present the result of the minimum variance analysis of magnetic fields. Here the $+L$ direction has a sunward component and we choose the polarity of the N direction according to the spacecraft velocity direction in the Mars rest frame in the same manner as *Halekas et al.* [2009], assuming that the spacecraft is overtaking the current sheet. The validity of this assumption will be checked by comparing the spacecraft velocity and ion bulk velocities in the current sheet normal direction. We find a bipolar variation in the intermediate variance B_M field, which is a characteristic signature of a crossing of Hall magnetic fields. We observe the B_L reversal from negative to positive values, negative-then-positive B_M bipolar signature, and positive B_N component. This pattern is consistent with a crossing sunward of the X line with type 3 polarity (Figure 1).

Additionally, electron distributions exhibit another signature consistent with the crossing sunward of the X line. In the electron pitch angle distributions during the current sheet crossing (Figure 2g), we first observe one-sided loss cones on the parallel side at 19:17:24–19:17:36, then two-sided loss cones with suppressed hot electron fluxes (see also Figure 2f) at 19:17:36–19:18:32, and finally one-sided loss cones on the antiparallel side at 19:18:32–19:19:04. This signature is consistent with a crossing of the closed field region between the two open field regions [*Harada et al.*, 2015a]. The closed field line topology is indicative of reconnected field lines on the Marsward (sunward) side of the X line.

Next we look at the ion measurements (Figures 2h–2j) to investigate the ion flows in the current sheet. We observe the positive enhancement of V_L for H^+ ions up to ~20 km/s during the current sheet crossing (Figure 2i). This sunward flow enhancement is consistent with the expected direction of the reconnection outflow for a crossing sunward of the X line. Meanwhile, the O^+ and O_2^+ ion velocities show only slight deviation toward $+V_L$ with no prominent sunward flows. The inverse dependence of ion acceleration on mass in the ion diffusion region was previously predicted by simulations [*Markidis et al.*, 2011; *Liu et al.*, 2015] and observed in the terrestrial and Martian magnetotails [*Liu et al.*, 2015; *Harada et al.*, 2015a]. According to these studies, the smaller acceleration of heavy ions compared to protons suggests that these heavy ions are still unmagnetized within the large heavy ion diffusion region and they are not yet fully accelerated toward the outflow direction at the observed location.

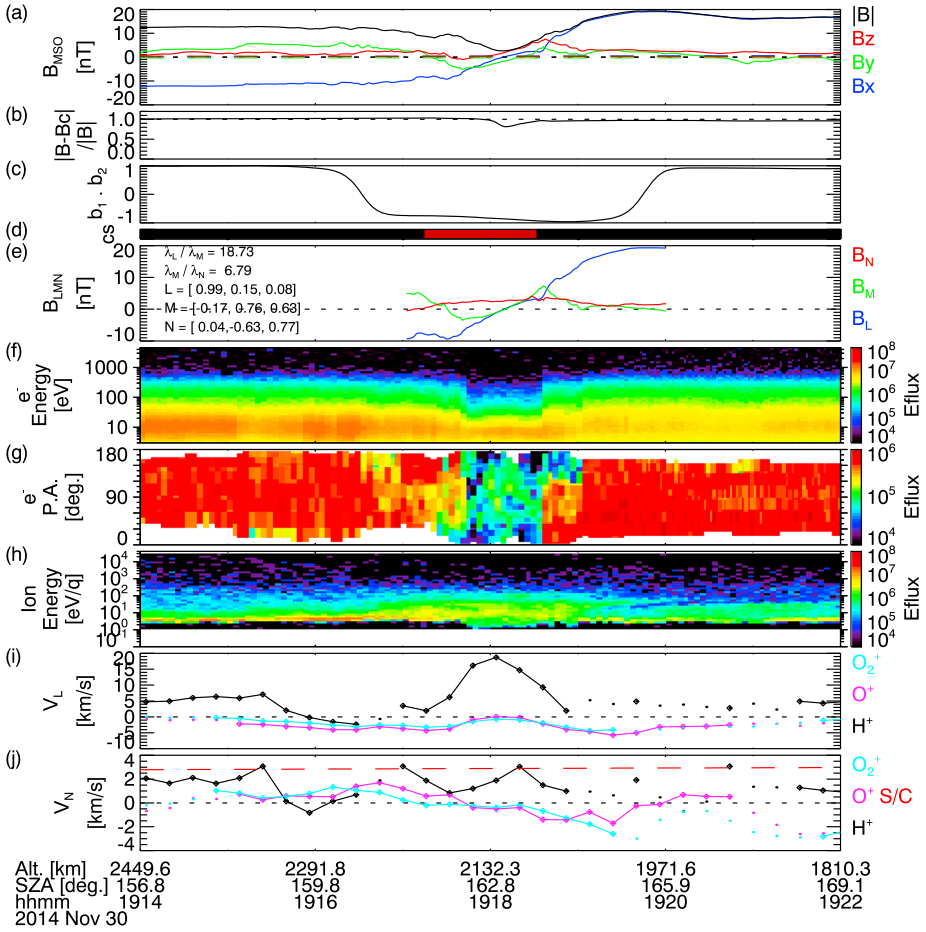

Figure 2. MAVEN observations on 30 November 2014 of (a) magnetic field in the MSO frame, (b) ratio of induced field to total field (1 = purely induced and 0 = purely crustal), (c) dot product, $\mathbf{b}_1 \cdot \mathbf{b}_2$, where $\mathbf{b}_1$ is the normalized vector of average magnetic field from t = −150 s to −45 s and $\mathbf{b}_2$ is that from t = +45 s to t = +150 s, (d) current sheet flag identified by an automated procedure (see section 5.1 for detail), (e) magnetic field in the minimum variance LMN coordinates, (f) electron energy spectra in units of differential energy flux (Eflux) of eV/cm^2/s/st/eV, (g) pitch angle distributions of 100–1000 eV electrons, (h) energy spectra of all ion species, and (i) *L* and (j) *N* component of bulk velocities for H^+, O^+, and O_2^+ ions in the Mars rest frame. The spacecraft altitude, solar zenith angle, and time in UT are indicated in the text label. The dashed lines in Figure 2a show the crustal magnetic field, $\mathbf{B}_c$, computed from the spherical harmonic model [*Morschhauser et al.*, 2014]. The MVA eigenvalue ratios and the maximum (*L*), intermediate (*M*), and minimum (*N*) variance directions in MSO are noted in Figure 2e. The polarity of the *N* direction is chosen according to the spacecraft MSO velocity based on the overtaking spacecraft assumption (see Figure 1 for the choice of the LMN polarity). In Figures 2i and 2j, the ion velocity data points are shown in diamonds and are connected by solid lines if the velocity measurement is relatively reliable, i.e., the main population of each species is well within the unblocked field of view and has good counting statistics, whereas the data points shown in unconnected dots represent less reliable velocity measurements when the main beam is close to the edge of the field of view or the density is too low (see section 3 for detail). The red dashed line in Figure 2j denotes the *N* component of the spacecraft velocity.

Figure 2j shows the *N* component of the ion velocities and spacecraft velocity in the Mars rest frame. We observe the ion V_N for the three major species consistently smaller than the spacecraft velocity throughout the current sheet crossing. This implies that the fast-moving spacecraft crossed the nearly stationary current sheet. Therefore, using the spacecraft velocity in the Mars rest frame to choose the polarity of the *N* direction would be appropriate for this event.

In short, the Hall magnetic field polarity, ion velocities, and electron distributions shown in Figure 2 are consistent with the expected signatures of a reconnecting current sheet crossed by a moving spacecraft.

4.2. Crossing Tailward of the X Line

Figure 3 presents a Hall magnetic field crossing tailward of the X line in the induced tail current sheet. We observe a large rotation (Figure 3c) of the induced-dominant fields (Figure 3b). The polarity of the observed

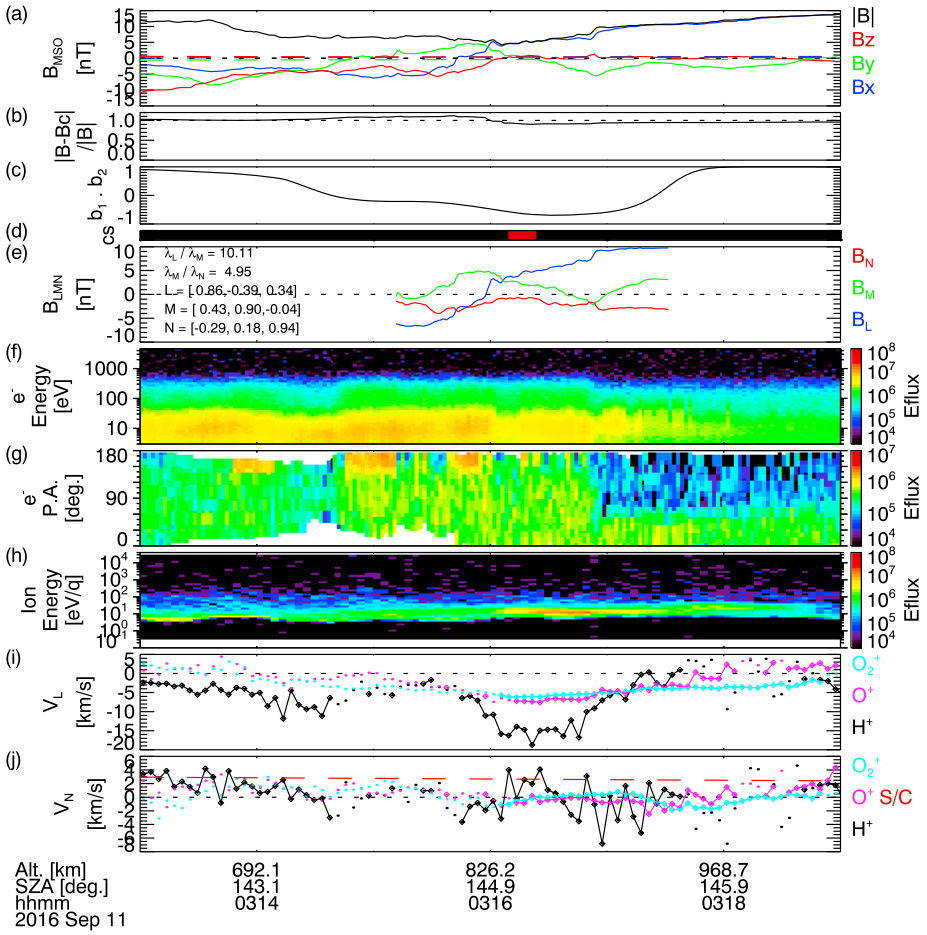

Figure 3. MAVEN observations on 11 September 2016 in the same format as Figure 2.

Hall fields based on the overtaking spacecraft assumption (Figure 3e) corresponds to a type 4 crossing tailward of the X line (Figure 1). Electron pitch angle distributions show intermittent, antiparallel field-aligned beams before the current sheet crossing, isotropic distributions at 03:16–03:17 during the crossing, and parallel field-aligned beams after the crossing (Figure 3g). The isotropic electron distributions suggest that the field lines are disconnected from the collisional atmosphere. Meanwhile, we observe tailward flow (negative V_L) enhancements of H^+, O^+, and O_2^+ ions during the crossing (Figure 3i). The H^+ V_L decreases down to −20 km/s, while the heavier ions exhibit smaller acceleration. Figure 3j shows that the spacecraft velocity in the *N* direction is consistently higher than the ion V_N, thereby validating the overtaking spacecraft assumption. The particle and magnetic field signatures observed in this event consistently suggest a crossing tailward of the X line in a nearly stationary current sheet.

4.3. Reconnection Signatures in an Induced-Crustal Current Sheet

We also find some Hall magnetic field crossings in the vicinity of crustal magnetic fields. Figure 4 shows such an example. Before the current sheet crossing at ~14:10, the induced-to-total field ratio is larger than 0.5, while it becomes smaller than 0.5 after the crossing (Figure 4b). This indicates that the spacecraft traveled from the induced-dominant fields (draped IMF) on one side of the current sheet to the crustal-dominant fields on the other side. Figure 4e displays a Hall magnetic field signature with type 3 polarity (Figure 1). The ion V_L profiles show sunward flow enhancements for H^+, O^+, and O_2^+ ions during the current sheet crossing (Figure 4i). The electron pitch angle distributions exhibit parallel loss cones beforehand, two-sided loss cones during the crossing, and antiparallel loss cones afterward (Figure 4g), implying that the hot electrons get trapped on closed field lines by reconnection. All of the Hall magnetic field polarity, ion flow enhancements, and trapped electrons are consistent with a crossing sunward of the X line. We note that the larger positive spacecraft velocity in the *N* direction than the ion V_N (Figure 4j) suggest that the spacecraft crossed the current sheet

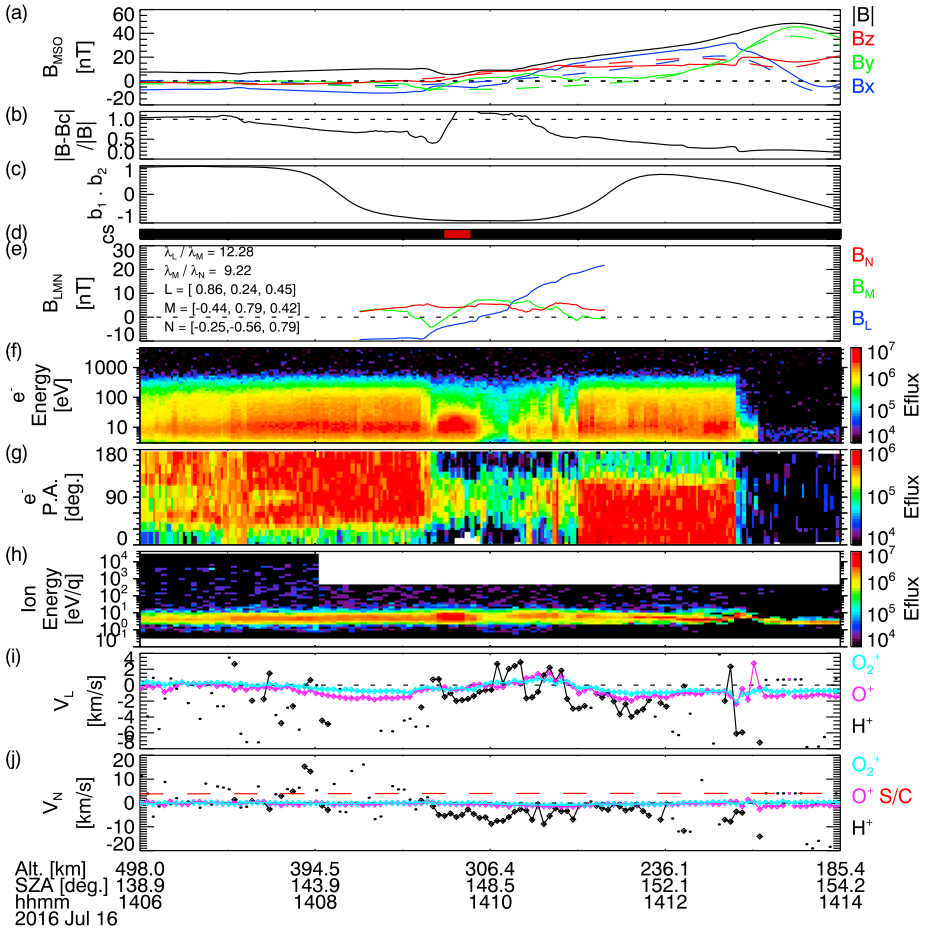

Figure 4. MAVEN observations on 16 July 2016 in the same format as Figure 2.

toward the +*N* direction as illustrated in Figure 1. These observations suggest that magnetic reconnection takes place in the current sheet formed between the draped IMF and the Martian crustal field.

4.4. Crossing of a Current Sheet Overtaking the Spacecraft

In Figure 5, we present another Hall magnetic field event observed near the apoapsis of the MAVEN orbit to demonstrate that the overtaking spacecraft assumption may not always be valid. If we choose the polarity of the *N* direction based on the overtaking spacecraft assumption, the observed Hall magnetic fields are consistent with a crossing tailward of the X line with type 4 polarity (Figures 1 and 5e). However, the ion velocities in the *N* direction are considerably higher than the *N* component of the spacecraft velocity throughout the interval (Figure 5j). If we assume that the overall current sheet structure convected with these ions, the current sheet would overtake the more slowly moving spacecraft. In this case, we need to flip the signs of the *N* and *M* directions when comparing the observed magnetic field time profile to that predicted in Figure 1. By reversing the signs of the B_N and B_M profiles, we now find that the observed Hall fields correspond to a type 3 crossing sunward of the X line. Furthermore, we observe a sunward flow enhancement in H^+ V_L at 15:15–15:18 (Figure 5i) and two-sided loss cones at 15:17–15:18 (Figure 5g), both of which are indicative of a crossing sunward of the X line. Based on these observations, we would conclude that this event is consistent with a reconnecting current sheet overtaking the spacecraft on the sunward side of the X line.

5. Statistical Survey

Here we conduct a comprehensive survey on reconnection signatures in the Martian magnetotail. We first identify Hall magnetic field crossings and then look at ion velocity data during these events. The method

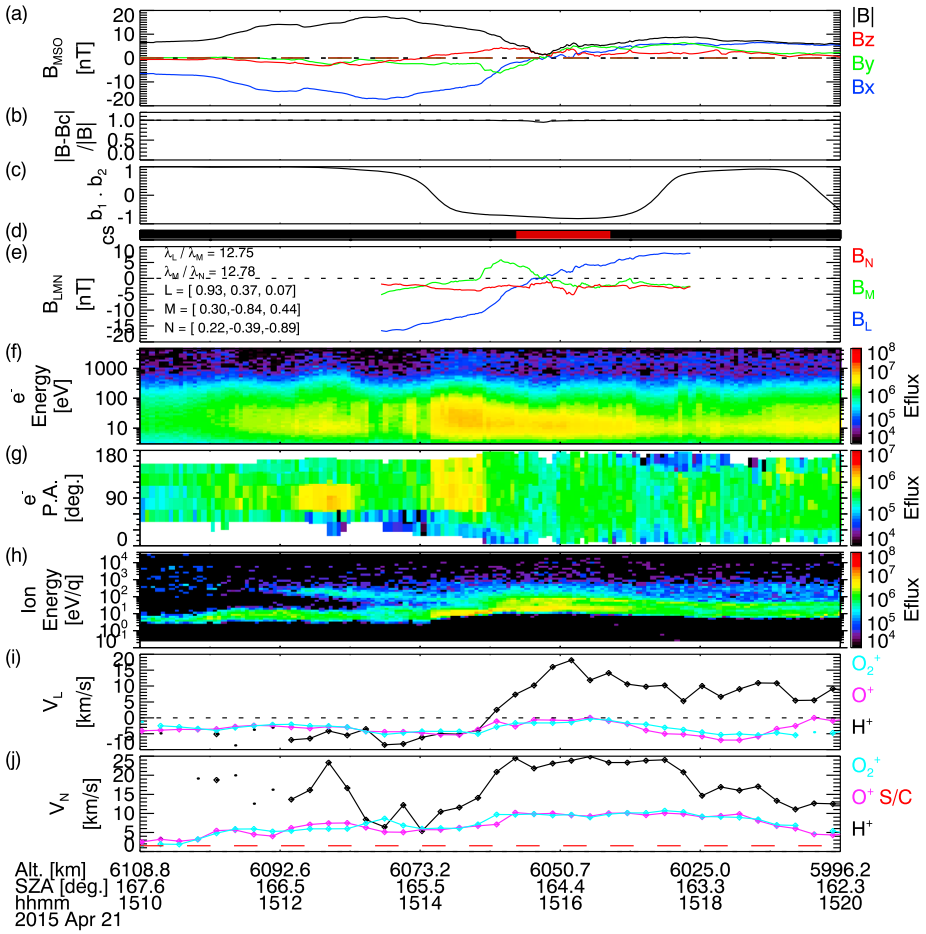

Figure 5. MAVEN observations on 21 April 2015 in the same format as Figure 2.

to produce a statistical data set of Hall field events is twofold: (i) identify current sheet crossings (based on *Halekas and Brain* [2010]) and (ii) identify Hall magnetic field signatures in the current sheet crossings (based on *Halekas et al.* [2009]).

5.1. Identifying Current Sheet Crossings

To efficiently and reliably identify current sheet crossings from the large volume of MAVEN data, we utilize an automated procedure adapted from the methodology originally developed for MGS data by *Halekas and Brain* [2010]. The algorithm searches for a typical signature of a current sheet crossing, namely, a dip in magnetic field strength accompanied by a large magnetic field rotation, as follows: For each time step of 1 s resolution MAG data, we compute the average magnetic field beforehand, $\mathbf{B}_1$, from $-150\ \mathrm{s} < t < -45\ \mathrm{s}$ and that afterward, $\mathbf{B}_2$, from $+45\ \mathrm{s} < t < +150\ \mathrm{s}$. If the dot product between their normalized vectors, $\mathbf{b}_1 \cdot \mathbf{b}_2$, is less than −0.5 (which corresponds to field rotation > 120°), and the field magnitude at the time step is less than 75% of the average magnitude in the $-150\ \mathrm{s} < t < -75\ \mathrm{s}$ and $+75\ \mathrm{s} < t < +150\ \mathrm{s}$ windows, we set a current sheet flag to be 1. Of these tentatively identified current sheet flags, we reset the flag to be 0 if (i) $|\mathbf{B}_1| < 5$ nT or $|\mathbf{B}_2| < 5$ nT to eliminate turbulent magnetic field rotation in the plasma sheet and to ensure a lobe-to-lobe crossing or (ii) the induced-to-total field ratio, $|\mathbf{B} - \mathbf{B}_c|/|\mathbf{B}|$, is less than 0.5 on each side to eliminate magnetic field rotation of purely crustal origin. Finally, we identify an individual current sheet crossing if the flag lasts for at least 12 s, thereby eliminating large-amplitude turbulent magnetic fields. Examples of the induced-to-total field ratio, dot product of normalized field vectors, and final current sheet flag are shown in Figures 2b–2d, 3b–3d, 4b–4d, and 5b–5d. We note that these criteria are optimized to find relatively thin current sheets with quick crossings shorter than ∼300 s. By applying this procedure to the MAVEN data from the 2332 tail crossing orbits (see section 3), we identified 776 current sheet crossings in 676 unique orbits (note that a single orbit may include multiple current sheet crossings).

5.2. Identifying Hall Magnetic Field Events

We visually searched the identified 776 current sheet crossings for bipolar out-of-plane field (B_M) signatures, resulting in finding 94 events. Of these 94 bipolar B_M events, we rejected 21 events with poor intermediate-to-minimum eigenvalue ratios ($\lambda_M/\lambda_N < 4$). We eliminated other 35 events with uncertain normal field polarities ($|\langle B_N \rangle| < 0.5$ nT or $|\langle B_N \rangle|/\delta B_N < 2$, where $\langle B_N \rangle$ and δB_N are the mean and standard deviation of the minimum variance component, respectively). We note that the elimination of small B_N events may result in missing small reconnection rate events and selecting only relatively intense reconnection events. Of the remaining 38 events, 34 have magnetic field variations consistent with Hall fields and only 4 have polarities inconsistent with Hall fields. Note that out of 8 possible combinations of (B_L reversal (positive to negative/negative to positive), bipolar B_M (positive to negative/negative to positive), B_N sign (positive/negative)), 4 combinations shown in Figure 1 are consistent with the Hall field and the other 4 patterns are inconsistent with the expected Hall field signatures. If the observed bipolar B_M signatures originated merely from random field variations, we would expect roughly the same chances of observing the consistent and inconsistent polarities. The overwhelming predominance of magnetic field polarities consistent with Hall fields suggests that the identified bipolar signatures are indeed generated by the Hall current system, which is in agreement with the previous study based on MGS data [*Halekas et al.*, 2009]. Basic properties of the identified Hall magnetic field events are compiled in Table 1.

5.3. Direction of the X Line Location

We applied two methods to determine the *LMN* polarity: (i) assumed that the spacecraft overtook the current sheets and (ii) analyzed the ion V_N data to infer the relative motion between the spacecraft and the current sheets. In the first approach, we found 16 events with Hall field polarities consistent with crossings sunward of X lines (types 1 and 3 in Figure 1) and 18 with polarities consistent with crossings tailward of X lines (types 2 and 4 in Figure 1) as listed in the "Hall B polarity" column of Table 1. The results using the second method are denoted in parentheses in the same column. For 19 of 34 events, the V_N profiles of H^+, O^+, and O_2^+ ions are consistently lower than the spacecraft normal velocity, validating that the spacecraft overtakes the current sheet. For only one event on 21 April 2015 shown in Figure 5, we observe positive ion V_N higher than the spacecraft normal velocity for the three species throughout the crossing (the current sheet overtaking the spacecraft), and the polarity result without ion V_N is reversed. For the remaining 14 events, the V_N profiles of the three ion species are not consistently higher or lower than the spacecraft normal velocity ("unclear") or reliable ion velocity measurements are not available during the crossings ("not available"), and we cannot confirm the validity of the overtaking spacecraft assumption. We do note that the breakdown of the overtaking spacecraft assumption reverses the expected direction of the X line location, but it does not affect the classification of bipolar B_M events consistent or inconsistent with the Hall field. Having seen that the spacecraft overtakes the current sheet in the majority of the events and that the overtaking current sheet event is rare, we hereafter look at statistics of the Hall field events by separating them into two groups, crossings sunward/tailward of X lines, according to the Hall field polarity results based on the overtaking spacecraft assumption.

The "Ion V_L enhancement?" column in Table 1 shows the presence of sunward/tailward enhancements of ion V_L for at least one species of available velocity measurements during the crossings or the absence thereof. Of the 16 crossings sunward of X lines based on the Hall field polarity, we found six with sunward V_L enhancements, zero with tailward V_L enhancements, eight with no clear sunward or tailward flow enhancements, and two with no available ion velocities. Of the 18 crossings tailward of X lines, we found 1 with sunward V_L enhancements (the 2015–04–21 event), 13 with tailward V_L enhancements, 3 with no clear sunward or tailward flow enhancements, and 1 with no available ion velocities. Remarkably, the majority of the events (19 out of 31 events with available ion velocity measurements) exhibit ion flow enhancement directions consistent with the Hall field polarity results based on the overtaking spacecraft assumption. Only one event on 21 April 2015 shows the flow enhancement opposite to the expected direction, and this event corresponds to the current sheet overtaking the spacecraft as demonstrated in Figure 5. Finally, we note that we did not find any expected sunward/tailward ion flow enhancements for about one third of the Hall field events (11 of 31), which will be discussed in section 6.

Next we compare the ion flow enhancements in the Hall field events to ion velocity profiles across "nominal" current sheets. Figure 6 shows a superposed epoch analysis of B_L and V_L for H^+, O^+, and O_2^+ ions during the current sheet crossings and Hall field events. Here the time from the current sheet center is normalized by

Table 1. Event List of Hall Magnetic Field Crossings

Date (YYYY–MM–DD)	Start Time (hh:mm:ss)	End Time (hh:mm:ss)	X_{MSO} (R_M)	ρ_{MSO} (R_M)	λ_M/λ_N	$\lvert\langle B_N\rangle\rvert$ $/\delta B_N$	Peak $\lvert B_M\rvert$ $/\lvert B_{L,lobe}\rvert$	$\lvert\langle B_N\rangle\rvert$ $/\lvert B_{L,lobe}\rvert$	Hall B Polarity (Including Ion V_N)	Ion V_L Enhancement?
2014–11–30	19:17:02	19:20:01	−1.56	0.48	6.8	2.08	0.37	0.14	Sunward (sunward)	Sunward
2014–12–02	08:13:10	08:15:08	−1.28	0.27	26.8	2.98	0.66	0.17	Tailward (unclear)	No
2014–12–04	01:28:40	01:33:02	−1.33	0.14	4.7	5.40	0.28	0.41	Sunward (unclear)	Sunward
2014–12–04	19:40:51	19:44:09	−1.51	0.47	42.2	3.19	0.52	0.18	Tailward (unclear)	Tailward
2014–12–06	22:05:47	22:10:03	−1.49	0.64	8.6	2.18	0.37	0.12	Tailward (not available)	Not available
2014–12–07	12:03:55	12:07:47	−1.33	0.04	23.2	3.46	0.43	0.13	Tailward (tailward)	Tailward
2014–12–10	13:10:04	13:12:17	−1.43	0.84	11.2	2.05	0.47	0.14	Sunward (not available)	Not available
2014–12–23	13:08:26	13:12:56	−0.94	0.53	11.0	2.21	0.66	0.27	Sunward (sunward)	Sunward
2014–12–28	16:35:14	16:37:40	−1.08	0.83	14.9	3.13	0.42	0.17	Tailward (unclear)	Tailward
2014–12–29	10:55:48	10:58:04	−1.07	0.80	6.9	2.64	0.45	0.21	Sunward (sunward)	Sunward
2014–12–29	15:29:17	15:36:37	−1.07	0.75	6.1	2.85	0.42	0.28	Tailward (unclear)	Tailward
2015–01–01	21:28:10	21:30:44	−1.02	0.63	10.8	2.20	0.26	0.08	Sunward (unclear)	No
2015–02–09	19:57:47	19:59:58	−0.76	0.91	25.6	2.11	0.45	0.09	Sunward (sunward)	No
2015–03–23	06:06:08	06:08:29	−1.75	0.94	4.3	2.94	0.37	0.22	Tailward (unclear)	Tailward
2015–04–21	15:13:26	15:17:52	−2.68	0.74	12.8	3.93	0.37	0.22	Tailward (sunward)	Sunward
2015–08–09	06:38:06	06:39:56	−0.70	0.84	5.3	2.65	0.36	0.19	Sunward (sunward)	Sunward
2015–08–21	14:45:08	14:49:18	−1.07	0.72	6.2	2.62	0.34	0.15	Sunward (unclear)	No
2015–09–13	10:24:32	10:28:37	−1.52	0.31	10.0	2.36	0.25	0.08	Sunward (unclear)	No
2015–09–26	03:53:54	03:57:50	−1.82	0.10	7.3	3.89	0.28	0.18	Sunward (not available)	Not available
2015–09–27	06:59:19	07:04:04	−1.45	0.50	26.5	2.65	0.48	0.12	Sunward (sunward)	No
2015–09–29	22:53:59	22:57:36	−1.77	0.22	9.1	2.08	0.43	0.20	Tailward (tailward)	No
2016–01–24	19:35:03	19:37:28	−0.76	0.89	17.1	4.45	0.24	0.13	Tailward (tailward)	Tailward
2016–03–20	08:11:56	08:16:22	−1.15	0.72	8.8	4.20	0.39	0.23	Sunward (sunward)	No
2016–03–20	12:56:01	12:59:11	−1.66	0.29	16.3	3.77	0.38	0.17	Tailward (tailward)	Tailward
2016–03–29	03:47:59	03:50:25	−1.90	0.70	78.1	2.17	0.49	0.06	Tailward (unclear)	No
2016–06–22	16:04:41	16:07:21	−0.77	0.93	9.3	2.17	0.38	0.13	Sunward (sunward)	No
2016–07–02	05:34:33	05:36:54	−0.85	0.81	5.2	5.47	0.18	0.20	Tailward (tailward)	Tailward
2016–07–16	14:08:30	14:11:19	−0.92	0.59	9.2	4.15	0.39	0.27	Sunward (sunward)	Sunward
2016–08–13	02:54:55	02:57:22	−0.63	0.88	5.6	5.38	0.28	0.31	Sunward (sunward)	No
2016–08–23	20:02:47	20:05:37	−1.12	0.68	13.0	4.30	0.48	0.30	Tailward (tailward)	Tailward
2016–08–25	22:52:36	22:55:40	−1.14	0.56	6.8	6.50	0.21	0.22	Tailward (tailward)	Tailward
2016–09–02	15:45:47	15:48:24	−1.13	0.57	17.0	3.00	0.52	0.16	Tailward (unclear)	Tailward
2016–09–11	03:15:11	03:17:32	−1.02	0.71	4.9	2.67	0.51	0.28	Tailward (tailward)	Tailward
2016–09–14	05:17:08	05:19:54	−0.95	0.79	6.1	4.01	0.51	0.40	Tailward (tailward)	Tailward

the current sheet half width W obtained from fitting of a Harris sheet field, $B_L = B_{L0}\tanh((t - t_0)/W)$, to the measured B_L profile during each current sheet crossing. It has been shown that magnetotail ion velocities are dependent on the distance from Mars [e.g., *Nilsson et al.*, 2010, 2012]; therefore, we analyze the events in three different X_{MSO} ranges: $-3R_M < X_{MSO} < -1.5R_M$, $-1.5R_M < X_{MSO} < -1R_M$, and $-1R_M < X_{MSO} < 0$. The thick black lines indicate the medians of all the identified current sheets in each X_{MSO} range, representing the nominal profiles, whereas the dashed lines show the upper and lower quartiles. We also show the median time profiles from the Hall field events in blue lines for crossings sunward of X lines and in red lines for crossings tailward of X lines. The nominal V_L profiles (black lines) demonstrate that ions are accelerated tailward (toward negative V_L) around current sheets as they travel downtail (Figure 6 (right to left columns), note that the y ranges vary for different distances). We observe positive deviations of the blue lines above the nominal levels during the crossings, indicating that sunward flow enhancements are likely to be observed during crossings sunward of X lines. Meanwhile, the red lines tend to display dips below the nominal levels, namely, tailward

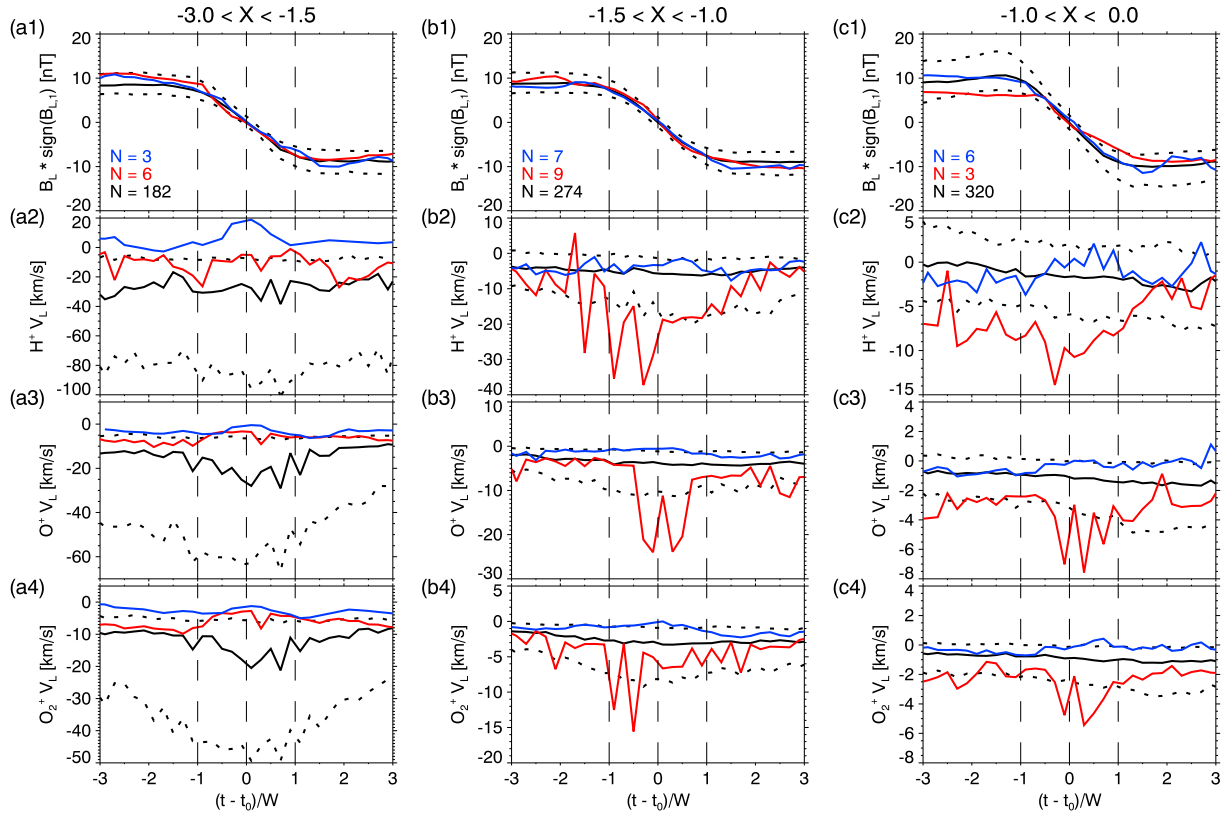

Figure 6. Superposed epoch analysis of L components of (a1) magnetic field, (a2) H^+, (a3) O^+, and (a4) O_2^+ ion velocities during the identified current sheet and Hall field crossings in $-3R_M < X_{MSO} < -1.5R_M$, (b1–b4) in $-1.5R_M < X_{MSO} < -1R_M$, and (c1–c4) in $-1R_M < X_{MSO} < 0$. The thick black lines show medians of the total current sheet crossings, and the dashed lines indicate their upper and lower quartiles. The blue (red) lines show medians of Hall magnetic field events with crossings sunward (tailward) of X lines. The time is normalized by the half width, W, of Harris sheet fitting, $B_L = B_{L0}\tanh((t - t_0)/W)$. The B_L profile is multiplied by the sign of B_L on the beginning side to ensure positive-to-negative reversals.

flow enhancements during crossings tailward of X lines, except in the most distant region at $-3R_M < X_{MSO} < -1.5R_M$ (Figures 6a2–6a4). We note that the nominal flows are expected to be asymmetric with fast, tailward flows in the $+E$ hemisphere and much slower flows in the $-E$ hemisphere [*Dubinin et al.*, 2013]. As seen later in section 5.4, the Hall field events are preferentially observed in the $-E$ hemisphere. This could explain the slower tailward flows than the median flows in Figures 6a2–6a4. Though the relation between the Hall field polarity and the ion flow deviation from the nominal conditions appears to be complex in the most distant tail region, we would conclude that the average ion flow profiles are in general agreement with the expected directions of X line locations based on the Hall field polarity measurements.

Here we conduct another test on the consistency of the Hall magnetic fields and ion flows by reconstructing the quadrupole structure of the Hall magnetic field B_M based on the combination of the measured B_L and ion V_L in a similar manner to the terrestrial magnetotail studies [e.g., *Eastwood et al.*, 2010]. Figure 7 shows scatterplots of ΔB_M as a function of sign-adjusted B_L and ion ΔV_L, where ΔB_M is the B_M deviation from the average value during the crossing to account for a nonzero guide field and ΔV_L represents V_L subtracted by the value averaged in two 150 s time windows just before and after the crossing interval to account for a nonzero background flow. The B_L sign is adjusted to the geometry of types 3 and 4 in Figure 1, in which L, M, and N correspond to X_{GSM}, Y_{GSM}, and Z_{GSM} of the Geocentric Solar Magnetospheric coordinate system in the terrestrial magnetotail. In this geometry, the Hall magnetic field structure predicts positive B_M in the $V_L * B_L > 0$ quadrants, whereas negative B_M is expected in the $V_L * B_L < 0$ quadrants. In the H^+ ion plot (Figure 7a), although the red and black circles are considerably mixed near $\Delta V_L \sim 0$, we do find the expected quadrupole pattern with more black circles in the top right and bottom left quadrants and with more red circles in the top left and bottom right quadrants. Meanwhile, we do not see as clear patterns as that of H^+ ions in the O^+ and O_2^+ ion velocities (Figures 7b and 7c). These observations suggest that lighter species provide better indicators of reconnection outflows in the ion diffusion regions.

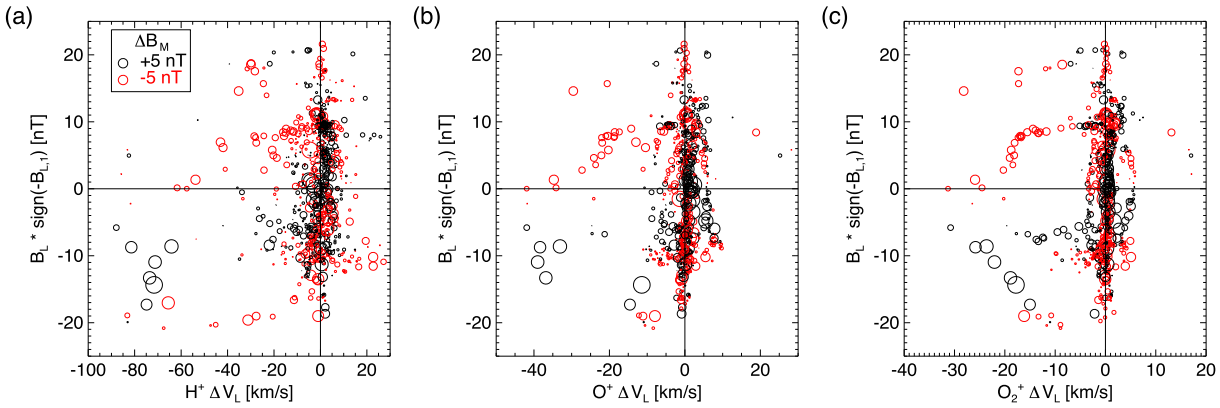

Figure 7. Out-of-plane magnetic field deviation ΔB_M as a function of B_L and ΔV_L for (a) H^+, (b) O^+, and (c) O_2^+ ions. For types 1 and 2 with positive-to-negative B_L reversals (Figure 1), the sign of B_L is flipped so that the geometry matches that of types 3 and 4 (in this geometry L, M, and N correspond to X_{GSM}, Y_{GSM}, and Z_{GSM} of the terrestrial magnetotail reconnection). The size of the circles represents $|\Delta B_M|$.

5.4. Spatial Distributions

We now examine spatial distributions of the reconnection events. Figure 8a shows cylindrical MSO distributions of the 776 identified current sheet crossings and 34 Hall field events as well as the directions of the observed ion flow enhancements. Both the identified current sheet crossings and Hall field events are not uniformly distributed over the sampled area. Most of the Hall field events are observed either close to Mars (e.g., $X_{MSO} > -1.2R_M$) or close to the tail center (e.g., $\rho_{MSO} < 0.5R_M$), although we do find the Hall field event in the distant tail as far as $X_{MSO} \sim -2.7R_M$ (the 2015–04–21 event). Figure 8b shows the observation likelihood of the Hall field signatures in the current sheet crossings as a function of X_{MSO}. We note that the X_{MSO} range between $-2.5R_M < X_{MSO} < -2R_M$ has been poorly sampled by MAVEN, and it is difficult to evaluate the observation likelihood in this region. We observe a high likelihood of ~6% at $-2R_M < X_{MSO} < -1R_M$, suggesting the preferred location of tail reconnection around $\sim 1-2R_M$ downstream from Mars.

Figure 9a shows the Y_{MSE}-Z_{MSE} distributions of the current sheet crossings and Hall field events. The conversion into MSE coordinates is conducted for 32 Hall field events with available upstream parameters (see section 3). We observe more Hall field events in the $-E$ hemisphere ($Z_{MSE} < 0$) compared to the $+E$ hemisphere ($Z_{MSE} > 0$), while the current sheet crossings are distributed throughout the wake. We note that this asymmetry cannot be explained by biased sampling; the Y_{MSE}-Z_{MSE} plane is more or less uniformly sampled by MAVEN (Figure 9b). The $\pm E$ hemispheric asymmetry can be clearly seen in the Z_{MSE} distribution of the observation likelihood of the Hall field events in the current sheet crossings (Figure 9c). The Hall field signatures are observed in ~7% of the identified current sheets at $Z_{MSE} < -0.5R_M$, while no Hall field event is found at $Z_{MSE} > 0.5R_M$. The observation likelihood increases up to ~11% if we limit the spatial region to $-2R_M < X_{MSO} < -1R_M$ and $Z_{MSE} < -0.5R_M$. The prominent asymmetry suggests that the $-E$ hemisphere is strongly favored for the occurrence of magnetic reconnection in the near-Mars magnetotail.

We note that the upstream IMF directions used for the coordinate transformation from MSO to MSE are estimated from orbit-average parameters, thereby smoothing out any rapid IMF variations with time scales shorter than the orbital period (~4.5 h). Such quick fluctuations and rotations in the upstream IMF might lead to inaccurate coordinate transformation in Figure 9. Nevertheless, as demonstrated in Figure 2 of *Harada et al.* [2015b], the smoothed IMF directions are proved to be useful to reconstruct the overall magnetotail configuration (e.g., the two lobe structure of B_x and $\pm E$ hemispheric asymmetry of magnetic field magnitude) in an average sense. Furthermore, as seen later in Figure 11f, interorbit IMF rotation angles are small (< 60°) for most of the orbits in our data set. Therefore, the uncertainty of the IMF direction due to short-term variations would not significantly alter the primary result of Figure 9, namely, the global asymmetry of occurrence of reconnection events between the $\pm E$ hemispheres.

The geographic distributions of the identified current sheet crossings and Hall field events are shown in Figure 10. We see that the Hall field events are distributed over a wide range of geographic coordinates, and they are not particularly correlated with the crustal field distribution. We note that some individual events do exhibit dominant crustal fields on one side of the current sheet (as seen in Figure 4). However, we find many

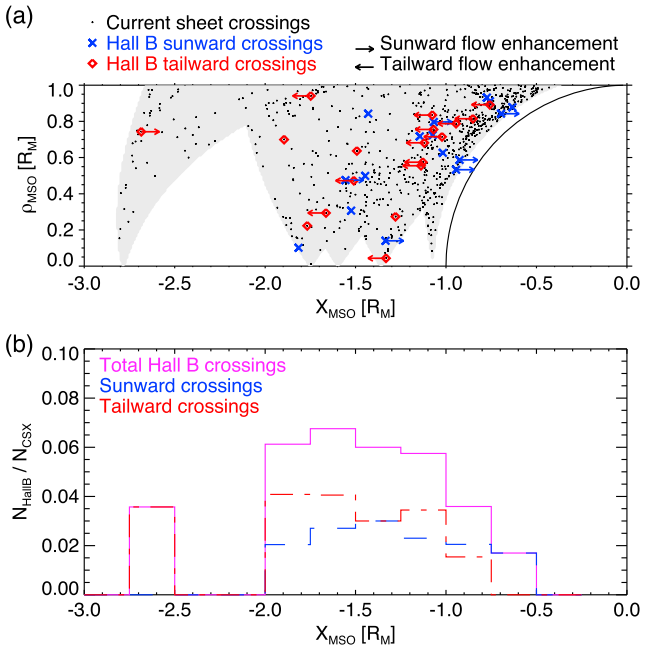

Figure 8. (a) Cylindrical MSO distributions of the identified current sheet crossings and Hall magnetic field events. The black dots represent current sheet crossings, the blue X signs show Hall field events with crossings sunward of X lines, and the red diamonds show Hall field events with crossings tailward of X lines. The Hall magnetic field events with sunward/tailward ion flow enhancements are indicated by rightward/leftward arrows. The gray area represents the spatial region sampled by MAVEN. (b) Likelihood of observing Hall magnetic field signatures in the identified current sheets as a function of X_{MSO}.

Hall field events distant from any strong crustal magnetic fields. From this data set, we cannot confirm a direct correlation between the crustal magnetic field distribution and the observation likelihood of reconnection signatures in the Martian magnetotail.

5.5. Dependence on Upstream Drivers

Here we investigate dependence of observations of tail reconnection signatures on a variety of upstream parameters. In Figure 11, the cyan solid lines show normalized histograms of the tail crossing orbits used in this paper, representing the "background" distributions of the upstream parameters. Meanwhile, the black dotted lines show the upstream parameter distributions for the current sheet crossings irrespective of Hall field signatures, and the magenta dashed lines show those for the Hall field events. By comparing the upstream parameter distributions of the Hall field events (magenta) to those of the tail crossing orbits (cyan) and current sheet crossings (black), we can examine whether or not the reconnection signatures are more likely to be observed in particular conditions.

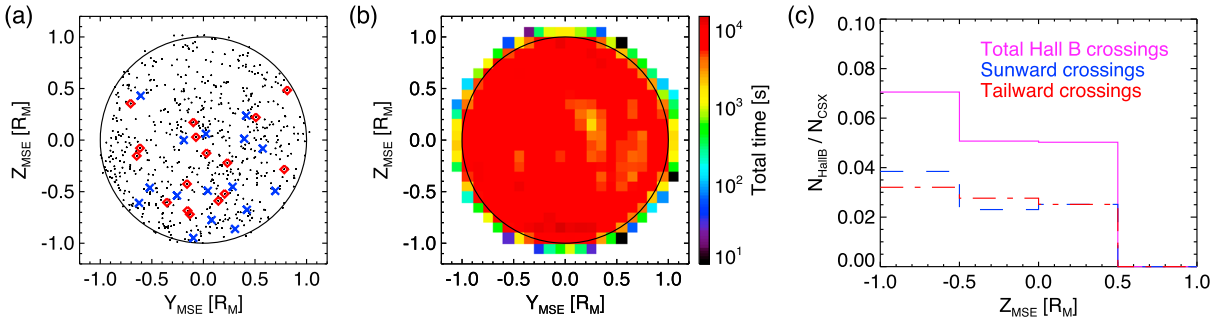

Figure 9. Y_{MSE}-Z_{MSE} distributions of (a) the identified current sheet crossings and Hall magnetic field events and (b) total sampling time. In Figure 9a, the black dots represent current sheet crossings, the blue X signs show Hall field events with crossings sunward of X lines, and the red diamonds show Hall field events with crossings tailward of X lines. (c) Likelihood of observing Hall magnetic field signatures in the identified current sheets as a function of Z_{MSE}.

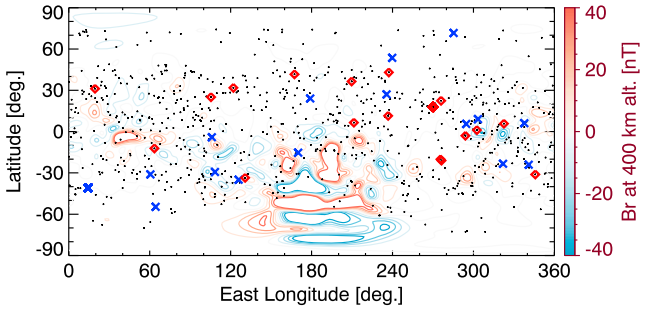

Figure 10. Geographic distributions of the identified current sheet crossings and Hall magnetic field events. The black dots represent current sheet crossings, the blue X signs show Hall field events with crossings sunward of X lines, and the red diamonds show Hall field events with crossings tailward of X lines. The contours show the radial component of crustal magnetic fields at 400 km altitude computed from the spherical harmonic model [*Morschhauser et al.*, 2014].

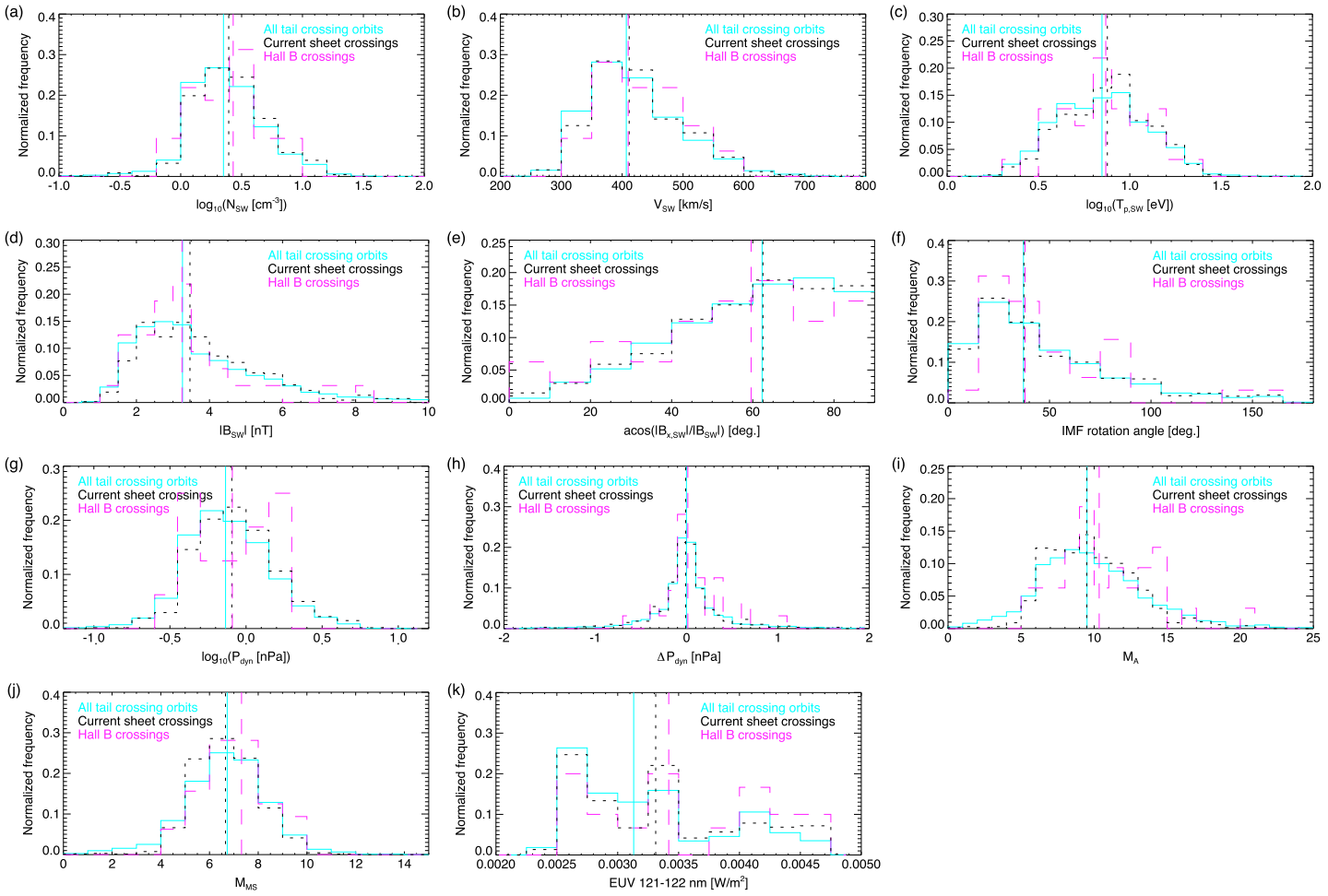

Figure 11. Normalized histograms of tail crossing orbits (cyan solid lines), current sheet crossings (black dotted lines), and Hall field events (magenta dashed lines) as functions of (a) solar wind density, (b) solar wind speed, (c) solar wind proton temperature, (d) IMF strength, (e) IMF cone angle, (f) IMF rotation angle during the tail passage, (g) solar wind dynamic pressure, (h) change in solar wind dynamic pressure during the tail passage, (i) Alfvén Mach number, (j) magnetosonic Mach number, and (k) EUV flux. The vertical lines show the medians. The upstream solar wind parameters (described in section 3) are available for 32 of 34 Hall field events, and the EUV flux is available for 30 of 34 events.

The upstream driver parameters that we examined include the solar wind density (Figure 11a), solar wind speed (Figure 11b), solar wind proton temperature (Figure 11c), IMF strength (Figure 11d), IMF cone angle (Figure 11e), IMF rotation angle during the tail passage (Figure 11f), solar wind dynamic pressure (Figure 11g), change in solar wind dynamic pressure during the tail passage (Figure 11h), Alfvén Mach number (Figure 11i), magnetosonic Mach number (Figure 11j), and EUV flux (Figure 11k). Overall, we did not find any strong dependence of the Hall field events on these parameters. For most of the parameters, we observe the Hall field distributions similar to those for the tail and current sheet crossings with nearly identical median values (indicated by the vertical lines). We do find weak dependence on the IMF cone angle (smaller angles are slightly favored as seen in Figure 11e), Alfvén and magnetosonic Mach numbers (higher Mach numbers are favored as seen in Figures 11i and 11j), and EUV flux (higher EUV fluxes are favored as seen in Figure 11k). However, even for these parameters, many Hall field events are found in both low and high conditions, suggesting that none of the examined upstream parameters represents a single, dominant factor controlling the occurrence of tail reconnection. We also looked at X_{MSO} locations of the Hall field events as functions of upstream parameters, resulting in finding no obvious correlation (not shown).

6. Discussion

In this section, we discuss the properties of the observed reconnection signatures in the context of previous observations at Mars and Venus. Although the expected and measured directions of ion flow enhancements agree for the majority of the Hall field events, we found no clear signatures of the expected sunward/tailward ion flow enhancements for about one third of the events. This could result from the large ion diffusion regions compared to the size of the Martian magnetotail. The ion gyroradii and inertial lengths can be comparable to, or even larger than, the scale lengths of the magnetic field structures in the Martian magnetotail (e.g., *Harada et al.* [2015a] estimated gyroradii and inertial lengths of O^+ and O_2^+ ions to be a few hundred kilometers, which are comparable to the local current sheet half thickness). Therefore, the ions within the large ion diffusion regions could still be unmagnetized and be decoupled from the reconnected field lines ejected away from the X line. The less effective outflow acceleration is expected to be more prominent for heavier ions [e.g., *Liu et al.*, 2015], which is indeed observed in the case studies (Figures 2–5). For some events, even H^+ ions do not exhibit any clear acceleration, implying that MAVEN could have crossed well within the H^+ diffusion region.

We also note that observations of sunward ion flows are not necessarily limited to the vicinity of current sheets in the Martian and Venusian magnetotails [*Harada et al.*, 2015b; *Kollmann et al.*, 2016], and these observations cannot be explained solely by direct acceleration via tail reconnection. Though *enhancements* of sunward flows during current sheet crossings provide a useful indicator of tail reconnection [*Dubinin et al.*, 2012b; *Zhang et al.*, 2012; *Harada et al.*, 2015a], a sunward ion flow *per se* should not be thought of as one-to-one correspondence to the occurrence of tail reconnection.

We determined the enhanced likelihood of observing reconnection signatures in the $-E$ hemisphere (Figure 9). This hemisphere coincides with magnetic field lines more tightly wrapped around the planet, which can be identified by the reversal of $B_{y,MSE}$, observed in the Martian tail [*Harada et al.*, 2015a] and Venusian tail [*Zhang et al.*, 2010; *Rong et al.*, 2014; *Xiao et al.*, 2016]. It has been proposed that the more tightly wrapped field configuration in the $-E$ hemisphere leads to, and/or results from, magnetic reconnection in thin tail current sheets [*Zhang et al.*, 2010, 2012; *Dubinin et al.*, 2013; *Xiao et al.*, 2016]. The MAVEN observations confirm that the Hall field signatures and associated ion flow enhancements are indeed more likely to be observed in the $-E$ hemisphere. It is also proposed that the reversed $B_{y,MSE}$ in the $-E$ hemisphere can be explained by an induced global magnetic field looping around the magnetotail [*Chai et al.*, 2016]. As a next step, it would be important to identify the ultimate drivers of the field line wrapping in the $-E$ hemisphere as well as the physical processes of current sheet thinning in the Martian and Venusian magnetotails.

The absence of notable correlation with upstream parameters (Figure 11) may seem surprising, given that the lobe magnetic field strength and ion fluxes in the Martian magnetotail are strongly controlled by upstream drivers such as the solar wind dynamic pressure [*Ferguson et al.*, 2005; *Lundin et al.*, 2008; *Harada et al.*, 2015b] and EUV flux [*Lundin et al.*, 2008]. The apparent lack of clear dependence on the upstream drivers implies that tail reconnection may be possible for a wide range of upstream parameters encountered by MAVEN. This interpretation is consistent with the Venus Express observations indicating that the magnetic field configuration in the Venusian tail, including the more tightly wrapped field lines in the $-E$ hemisphere, persists during both solar maximum and minimum [*Xiao et al.*, 2016]. As an alternative explanation for the lack of correlation

with individual upstream parameters, the occurrence of tail reconnection could depend on the combination of multiple parameters instead of a single parameter. Unfortunately, the 34 Hall field events identified so far do not provide sufficient statistics for a multiparameter analysis. We might be able to address this issue as the MAVEN data continue to be accumulated.

Finally, we discuss the occurrence frequency of magnetic reconnection in the Martian magnetotail. We note that the likelihood of observing the Hall field signatures in the identified current sheets (locally up to ~11% in the most preferred region) may not represent the effective duty cycle of tail reconnection (defined here as the fraction of time during which reconnection is active at one or multiple locations in the Martian magnetotail). This is because (i) we selected only relatively intense reconnection events with significant normal fields and (ii) we selected only relatively thin current sheets with quick crossings. Instead, we can obtain a robust lower limit of ~1.5% by taking into account that 34 unique events were found out of 2332 tail crossing orbits, indicating that reconnection is ongoing somewhere in the tail for at least 34/2332 ~ 1.5% of the time. This number should be considered as a very conservative estimate because MAVEN could have missed many reconnection structures that happened to be located far from the particular MAVEN orbit. Based on these estimates, we would infer a tail reconnection duty cycle on the order of ~1–10% or even higher. This implies that magnetic reconnection is an important process for the particle transport and rearrangement of the magnetic field topology in the Martian magnetotail.

7. Conclusions

We have investigated properties of reconnection signatures in the Martian magnetotail with MAVEN data. Having confirmed that the expected signatures of Hall magnetic fields and ion flow enhancements are found in several case studies, we performed a statistical survey by identifying current sheet crossings and Hall field events from the available MAVEN data set based on the previously developed methodology. For about two thirds of the identified Hall field events with available ion velocity data, the ion velocities exhibit flow enhancements in the directions consistent with those expected from the Hall field polarity. For the rest of the events, no clear enhancements in ion flow velocities are observed during the current sheet crossings, implying that ions could be still unmagnetized and decoupled from the reconnected field lines in the near-Mars magnetotail. The spatial distributions of the Hall field events (with a data gap between $-2.5R_M < X_{MSO} < -2R_M$) suggest that reconnection occurs preferentially in the $-E$ hemisphere of the near-Mars magnetotail at $-2R_M < X_{MSO} < -1R_M$, where magnetic field lines are more tightly wrapped around the planet. The Hall field events are distributed over a wide geographic area regardless of crustal magnetic field strengths. The reconnection signatures are found in current sheets with induced fields on both sides and with induced fields on one side and crustal fields on the other. Also, no strong dependence on upstream drivers has been identified. Based on the event statistics, we can infer that magnetic reconnection operates in the Martian magnetotail for ~1–10% of the time or even at a higher rate. These observations demonstrate that magnetic reconnection can play an important role in magnetotail dynamics at Mars.

Acknowledgments
The authors gratefully acknowledge support from the team members of the MAVEN mission. The research presented in this paper was funded by the NASA MAVEN Project and the French space agency CNES. MAVEN data are publicly available through the Planetary Data System (http://ppi.pds.nasa.gov/mission/MAVEN).

References

Beharrell, M. J., and J. A. Wild (2012), Stationary flux ropes at the southern terminator of Mars, *J. Geophys. Res.*, *117*, A12212, doi:10.1029/2012JA017738.

Brain, D., et al. (2010a), A comparison of global models for the solar wind interaction with Mars, *Icarus*, *206*(1), 139–151, doi:10.1016/j.icarus.2009.06.030.

Brain, D. A., A. H. Baker, J. Briggs, J. P. Eastwood, J. S. Halekas, and T.-D. Phan (2010b), Episodic detachment of Martian crustal magnetic fields leading to bulk atmospheric plasma escape, *Geophys. Res. Lett.*, *37*, L14108, doi:10.1029/2010GL043916.

Brain, D. A., R. J. Lillis, D. L. Mitchell, J. S. Halekas, and R. P. Lin (2007), Electron pitch angle distributions as indicators of magnetic field topology near Mars, *J. Geophys. Res.*, *112*, A09201, doi:10.1029/2007JA012435.

Briggs, J., D. Brain, M. Cartwright, J. Eastwood, and J. Halekas (2011), A statistical study of flux ropes in the Martian magnetosphere, *Planet. Space Sci.*, *59*(13), 1498–1505, doi:10.1016/j.pss.2011.06.010.

Chai, L., et al. (2016), An induced global magnetic field looping around the magnetotail of Venus, *J. Geophys. Res. Space Physics*, *121*(1), 688–698, doi:10.1002/2015JA021904.

Connerney, J., J. Espley, P. Lawton, S. Murphy, J. Odom, R. Oliversen, and D. Sheppard (2015), The MAVEN magnetic field investigation, *Space Sci. Rev.*, *195*(1–4), 257–291, doi:10.1007/s11214-015-0169-4.

DiBraccio, G. A., et al. (2015), Magnetotail dynamics at Mars: Initial MAVEN observations, *Geophys. Res. Lett.*, *42*(21), 8828–8837, doi:10.1002/2015GL065248.

Dubinin, E., and M. Fraenz (2015), Magnetotails of Mars and Venus, *Geophys. Monogr. Ser.*, *207*, 43–59, doi:10.1002/9781118842324.ch3.

Dubinin, E., M. Fraenz, A. Fedorov, R. Lundin, N. Edberg, F. Duru, and O. Vaisberg (2012a), Ion energization and escape on Mars and Venus, *Space Sci. Rev.*, *162*, 173–211, doi:10.1007/978-1-4614-3290-6_6.

Dubinin, E., M. Fraenz, J. Woch, T. L. Zhang, J. Wei, A. Fedorov, S. Barabash, and R. Lundin (2012b), Bursty escape fluxes in plasma sheets of Mars and Venus, *Geophys. Res. Lett.*, *39*(1), L01104, doi:10.1029/2011GL049883.

Dubinin, E., M. Fraenz, T. L. Zhang, J. Woch, Y. Wei, A. Fedorov, S. Barabash, and R. Lundin (2013), Plasma in the near Venus tail: Venus Express observations, *J. Geophys. Res. Space Physics*, *118*, 7624–7634, doi:10.1002/2013JA019164.

Dungey, J. W. (1961), Interplanetary magnetic field and the auroral zones, *Phys. Rev. Lett.*, *6*, 47–48, doi:10.1103/PhysRevLett.6.47.

Eastwood, J. P., and S. A. Kiehas (2015), Origin and evolution of plasmoids and flux ropes in the magnetotails of Earth and Mars, *Geophys. Monogr. Ser.*, *207*, 269–287, doi:10.1002/9781118842324.ch16.

Eastwood, J. P., T. D. Phan, M. Øieroset, and M. A. Shay (2010), Average properties of the magnetic reconnection ion diffusion region in the Earth's magnetotail: The 2001–2005 Cluster observations and comparison with simulations, *J. Geophys. Res.*, *115*, A08215, doi:10.1029/2009JA014962.

Eastwood, J. P., J. J. H. Videira, D. A. Brain, and J. S. Halekas (2012), A chain of magnetic flux ropes in the magnetotail of Mars, *Geophys. Res. Lett.*, *39*(3), L03104, doi:10.1029/2011GL050444.

Eastwood, J. P., D. A. Brain, J. S. Halekas, J. F. Drake, T. D. Phan, M. Oieroset, D. L. Mitchell, R. P. Lin, and M. Acuña (2008), Evidence for collisionless magnetic reconnection at Mars, *Geophys. Res. Lett.*, *35*, L02106, doi:10.1029/2007GL032289.

Eparvier, F. G., P. C. Chamberlin, T. N. Woods, and E. M. B. Thiemann (2015), The solar extreme ultraviolet monitor for MAVEN, *Space Sci. Rev.*, *195*(1), 293–301, doi:10.1007/s11214-015-0195-2.

Ferguson, B. B., J. C. Cain, D. H. Crider, D. A. Brain, and E. M. Harnett (2005), External fields on the nightside of Mars at Mars Global Surveyor mapping altitudes, *Geophys. Res. Lett.*, *32*(16), L16105, doi:10.1029/2004GL021964.

Halekas, J., E. Taylor, G. Dalton, G. Johnson, D. Curtis, J. McFadden, D. Mitchell, R. Lin, and B. Jakosky (2015), The solar wind ion analyzer for MAVEN, *Space Sci. Rev.*, *195*, 125–151, doi:10.1007/s11214-013-0029-z.

Halekas, J. S., and D. A. Brain (2010), Global distribution, structure, and solar wind control of low altitude current sheets at Mars, *Icarus*, *206*(1), 64–73, doi:10.1016/j.icarus.2008.12.032.

Halekas, J. S., et al. (2016), Structure, dynamics, and seasonal variability of the Mars-solar wind interaction: MAVEN solar wind ion analyzer inflight performance and science results, *J. Geophys. Res. Space Physics*, *121*, 547–578, doi:10.1002/2016JA023167.

Halekas, J. S., J. P. Eastwood, D. A. Brain, T. D. Phan, M. Oieroset, and R. P. Lin (2009), In situ observations of reconnection Hall magnetic fields at Mars: Evidence for ion diffusion region encounters, *J. Geophys. Res.*, *114*, A11204, doi:10.1029/2009JA014544.

Hara, T., K. Seki, H. Hasegawa, D. A. Brain, K. Matsunaga, M. H. Saito, and D. Shiota (2014), Formation processes of flux ropes downstream from Martian crustal magnetic fields inferred from Grad-Shafranov reconstruction, *J. Geophys. Res. Space Physics*, *119*, 7947–7962, doi:10.1002/2014JA019943.

Hara, T., et al. (2016), MAVEN observations of a giant ionospheric flux rope near Mars resulting from interaction between the crustal and interplanetary draped magnetic fields, *J. Geophys. Res. Space Physics*, *121*, 828–842, doi:10.1002/2016JA023347.

Harada, Y., et al. (2015a), Magnetic reconnection in the near-Mars magnetotail: MAVEN observations, *Geophys. Res. Lett.*, *42*, 8838–8845, doi:10.1002/2015GL065004.

Harada, Y., et al. (2015b), Marsward and tailward ions in the near-Mars magnetotail: MAVEN observations, *Geophys. Res. Lett.*, *42*, 8925–8932, doi:10.1002/2015GL065005.

Harada, Y., et al. (2016), MAVEN observations of energy-time dispersed electron signatures in Martian crustal magnetic fields, *Geophys. Res. Lett.*, *43*, 939–944, doi:10.1002/2015GL067040.

Jakosky, B. M., et al. (2015), The Mars Atmosphere and Volatile Evolution (MAVEN) mission, *Space Sci. Rev.*, *195*(1–4), 3–48, doi:10.1007/s11214-015-0139-x.

Kollmann, P., P. Brandt, G. Collinson, Z. Rong, Y. Futaana, and T. Zhang (2016), Properties of planetward ion flows in Venus' magnetotail, *Icarus*, *274*, 73–82, doi:10.1016/j.icarus.2016.02.053.

Liu, Y. H., C. G. Mouikis, L. M. Kistler, S. Wang, V. Roytershteyn, and H. Karimabadi (2015), The heavy ion diffusion region in magnetic reconnection in the Earth's magnetotail, *J. Geophys. Res. Space Physics*, *120*, 3535–3551, doi:10.1002/2015JA020982.

Lundin, R. (2011), Ion acceleration and outflow from Mars and Venus: An overview, *Space Sci. Rev.*, *162*(1–4), 309–334, doi:10.1007/s11214-011-9811-y.

Lundin, R., S. Barabash, A. Fedorov, M. Holmström, H. Nilsson, J.-A. Sauvaud, and M. Yamauchi (2008), Solar forcing and planetary ion escape from Mars, *Geophys. Res. Lett.*, *35*, L09203, doi:10.1029/2007GL032884.

Markidis, S., G. Lapenta, L. Bettarini, M. Goldman, D. Newman, and L. Andersson (2011), Kinetic simulations of magnetic reconnection in presence of a background o+ population, *J. Geophys. Res.*, *116*, A00K16, doi:10.1029/2011JA016429.

McFadden, J. P., et al. (2015), MAVEN SupraThermal and Thermal Ion Compostion (STATIC) instrument, *Space Sci. Rev.*, *195*(1–4), 199–256, doi:10.1007/s11214-015-0175-6.

Mitchell, D. L., et al. (2016), The MAVEN solar wind electron analyzer, *Space Sci. Rev.*, *200*(1), 495–528, doi:10.1007/s11214-015-0232-1.

Morschhauser, A., V. Lesur, and M. Grott (2014), A spherical harmonic model of the lithospheric magnetic field of Mars, *J. Geophys. Res. Planets*, *119*, 1162–1188, doi:10.1002/2013JE004555.

Niedner Jr., M. B., and J. C. Brandt (1978), Interplanetary gas. XXII—Plasma tail disconnection events in comets—Evidence for magnetic field line reconnection at interplanetary sector boundaries, *Astrophys. J.*, *223*, 655–670, doi:10.1086/156299.

Nilsson, H., E. Carlsson, D. A. Brain, M. Yamauchi, M. Holmström, S. Barabash, R. Lundin, and Y. Futaana (2010), Ion escape from Mars as a function of solar wind conditions: A statistical study, *Icarus*, *206*(1), 40–49, doi:10.1016/j.icarus.2009.03.006.

Nilsson, H., G. Stenberg, Y. Futaana, M. Holmström, S. Barabash, R. Lundin, N. J. T. Edberg, and A. Fedorov (2012), Ion distributions in the vicinity of Mars: Signatures of heating and acceleration processes, *Earth Planets Space*, *64*(2), 135–148, doi:10.5047/eps.2011.04.011.

Paschmann, G., M. Øieroset, and T. Phan (2013), In-situ observations of reconnection in space, *Space Sci. Rev.*, *178*(2–4), 385–417, doi:10.1007/s11214-012-9957-2.

Pritchett, P. L. (2001), Geospace environment modeling magnetic reconnection challenge: Simulations with a full particle electromagnetic code, *J. Geophys. Res.*, *106*(A3), 3783–3798, doi:10.1029/1999JA001006.

Rong, Z. J., S. Barabash, Y. Futaana, G. Stenberg, T. L. Zhang, W. X. Wan, Y. Wei, X.-D. Wang, L. H. Chai, and J. Zhong (2014), Morphology of magnetic field in near-Venus magnetotail: Venus express observations, *J. Geophys. Res. Space Physics*, *119*(11), 8838–8847, doi:10.1002/2014JA020461.

Russell, C. T. (2001), The dynamics of planetary magnetospheres, *Planet. Space Sci*, *49*, 1005–1030, doi:10.1016/S0032-0633(01)00017-4.

Russell, C. T., M. A. Saunders, J. L. Phillips, and J. A. Fedder (1986), Near-tail reconnection as the cause of cometary tail disconnections, *J. Geophys. Res.*, *91*(A2), 1417–1423, doi:10.1029/JA091iA02p01417.

Sonnerup, B. U. Ö., and L. J. Cahill (1967), Magnetopause structure and attitude from Explorer 12 observations, *J. Geophys. Res.*, *72*(1), 171–183, doi:10.1029/JZ072i001p00171.

Soobiah, Y. I., J. A. Wild, M. J. Beharrell, S. Barabash, R. J. Lillis, D. L. Mitchell, A. J. Coates, J. D. Winningham, and R. A. Frahm (2014), Properties of a large-scale flux rope and current sheet region on the dayside of Mars: MGS MAG/ER and MEX ASPERA-3 ELS observations, *Icarus*, *242*, 297–315, doi:10.1016/j.icarus.2014.08.019.

Southwood, D. J. (2015), Formation of magnetotails, *Geophys. Monogr. Ser.*, *207*, 197–215, doi:10.1002/9781118842324.ch12.
Ulușen, D., and I. Linscott (2008), Low-energy electron current in the Martian tail due to reconnection of draped interplanetary magnetic field and crustal magnetic fields, *J. Geophys. Res.*, *113*, E06001, doi:10.1029/2007JE002916.
Vech, D., G. Stenberg, H. Nilsson, N. J. T. Edberg, A. Opitz, K. Szegő, T. Zhang, and Y. Futaana (2016), Statistical features of the global polarity reversal of the Venusian induced magnetosphere in response to the polarity change in interplanetary magnetic field, *J. Geophys. Res. Space Physics*, *121*, 3951–3962, doi:10.1002/2015JA021995.
Xiao, S. D., T. L. Zhang, and W. Baumjohann (2016), Hemispheric asymmetry in the near-Venusian magnetotail during solar maximum, *J. Geophys. Res. Space Physics*, *121*, 4542–4547, doi:10.1002/2015JA022093.
Xu, S., et al. (2016), Deep nightside photoelectron observations by MAVEN SWEA: Implications for Martian northern hemispheric magnetic topology and nightside ionosphere source, *Geophys. Res. Lett.*, *43*, 8876–8884, doi:10.1002/2016GL070527.
Yamada, M., R. Kulsrud, and H. Ji (2010), Magnetic reconnection, *Rev. Mod. Phys.*, *82*, 603–664, doi:10.1103/RevModPhys.82.603.
Zhang, T. L., W. Baumjohann, J. Du, R. Nakamura, R. Jarvinen, E. Kallio, A. M. Du, M. Balikhin, J. G. Luhmann, and C. T. Russell (2010), Hemispheric asymmetry of the magnetic field wrapping pattern in the Venusian magnetotail, *Geophys. Res. Lett.*, *37*, L14202, doi:10.1029/2010GL044020.
Zhang, T. L., et al. (2012), Magnetic reconnection in the near Venusian magnetotail, *Science*, *336*(6081), 567–570, doi:10.1126/science.1217013.